Journal of Alloys and Compounds 768 (2018) 883–888

Contents lists available at ScienceDirect

Journal of Alloys and Compounds

journal homepage: http://www.elsevier.com/locate/jalcom

# Cation substitution inducing gap changes and covalent interaction flexibility enhancing second harmonic generation responses in $d^{10}$ metal chalcogenides

Jianian Cheng [a], Ming-Hsien Lee [b], Jun Zhang [a, *]

[a] School of Physics Science and Technology, Xinjiang University, Urumqi, Xinjiang 830046, China
[b] Department of Physics, Tamkang University, New Taipei 25137, Taiwan

ARTICLE INFO

*Article history:*
Received 11 April 2018
Received in revised form
10 July 2018
Accepted 28 July 2018
Available online 30 July 2018

*Keywords:*
Influence of cations
DFT
Electronic structure
NLO properties

ABSTRACT

Desiring a high-performance infrared (IR) material with a wide band gap and large second harmonic generation (SHG) response motivates the studies about the chemistry and electronic structure of microscopic structures. In this research, the covalence, electronic structure and mechanism of SHG effect for a typical IR system, $d^{10}$ metal chalcogenides with $AB_2S_4$ (A = Cd, Hg; B = Al, Ga) family, were systemically investigated. It reveals that the *dp* hybridization, size effect and the cation electronegativity induce the changes of band gaps. Besides the decrease of charge-transfer energy enlarging the SHG effect, we found that the strong covalent interaction between atoms is also beneficial to the SHG enhancement. More importantly, the nonlinear optical (NLO) functional units for superior IR performances were investigated, and the results show that IIIA-S functional units have strong covalent interaction and more priority on NLO properties. Furthermore, the electronic structures of sulfur in the compounds are susceptible to the type of cations, and consequently affect the NLO properties.



## 1. Introduction

Nonlinear optical (NLO) materials play an exceedingly crucial role in the development of solid-state lasers by frequency-doubling conversion technology [1–4]. In the past decades, many famous NLO materials applied in ultraviolet (UV) regions have been synthesized, such as borates, carbonates, and phosphates [5–7]. Recently, the first-principles method employed by Pan and Yang et al. proved that fluorooxoborates can be potential deep-UV NLO candidates mainly due to introducing excellent NLO active groups $(BO_xF_{4-x})^{(x+1)-}$ (x = 1, 2, 3) [8]. And a class of novel deep-UV NLO fluorooxoborates [9], have been successfully designed and synthesized. This design strategy can be expected in the exploration of infrared (IR) materials, which are urgent for commercialization. For IR region, weak interatomic bonds like in chalcogenides are beneficial to expand the transparent to IR region [10,11], therefore the relationship between microscopic structure and macroscopic properties will be different from oxides. Consequently, a better understanding of what kinds of microscopic building units are related to the NLO properties, and how do cations affect SHG effect was proven as a meaningful design for new functional materials.

Recently, the researches about IR materials also have made significant progress. The typical examples are $AgGaX_2$ (X = S, Se) [12] and $ZnGeP_2$ [13]. However, commercially available NLO materials in the IR ranges, two important atmospheric transparent windows (3–5 μm, 8–12 μm), are still limited. Therefore, great attention has been paid to searching novel IR materials with high laser damage thresholds (LDTs) and large NLO coefficients in these two ranges. Nevertheless, it is known that the larger band gap may be beneficial to generating high LDT, but results in small NLO coefficients ($d_{ij}$) [14]. We review the achievements in the exploration of new metal-chalcogenide NLO materials for the IR region [11,15], introducing alkali/alkaline-earth metals, IIIA metals, $d^{10}$ metals, and NLO active groups in the crystal structures [16], is available to obtain the potential IR materials, such as $Na_2Ge_2Se_5$ [17], $LiGaS_2$ [18], $LiInS_2$ [19], $Li_2CdGeS_4$ [20], $Li_2ZnSiS_4$ [21], $BaHgSe_2$ [22], and $Ba_3(BS_3)(SbS_3)$ [23].

Benefiting from their high performances and IR applications, metal chalcogenides are highly promising IR materials. Furthermore, metal chalcogenides with diamond-like structure, tetrahedral groups, and $d^{10}$ metal cations are preferential options for

* Corresponding author.
*E-mail address:* zhangjunxju@163.com (J. Zhang).

https://doi.org/10.1016/j.jallcom.2018.07.326
0925-8388/

design since they have inherently local non-centrosymmetry (NCS) that benefits to obtaining NLO materials [24]. Previous experimental measurements and *ab-initio* calculations show that the $d^{10}$ metal chalcogenides have large band gap and SHG response. In this work, we focus on $d^{10}$ metal chalcogenides $AB_2S_4$ (A = Cd, Hg; B = Al, Ga) family because they have a good balance between the band gap $E_g$ (circa = 3.0 eV) and the NLO coefficient $d_{ij}$ ($1 \times AgGaS_2$, $d_{36} = 13$ pm/V) [25,26], we studied the intrinsic mechanism for SHG response, and the structure-property relationship based on the density functional theory (DFT) [27,28]. Furthermore, the influence of $d^{10}$ metal cations on the electronic structure and SHG properties were also discussed. And the results show that $d^{10}$ metal cations have influences both on sulfur and overall optical properties by the hybridization with S-3*p* orbitals.

## 2. Methods and computational details

The first-principles calculations were performed under the DFT using the plane wave pseudopotential method in the CASTEP module [29]. In this work, the generalized gradient approximation (GGA) [30] of Perdew-Burke-Ernzerhof (PBE) [31] functional was adopted, the norm-conserving pseudopotentials (NCP) [32–34] were set up for all calculations of electronic structure and optical property. The energy cutoff of 720 eV for $CdAl_2S_4$, $CdGa_2S_4$, $HgAl_2S_4$ and $HgGa_2S_4$ was set to reach the convergence of the calculations. Pseudo atomic calculations were performed based on the following orbital electrons as valence electrons: Cd $4d^{10}$ $5s^2$, Hg $5d^{10}$ $6s^2$, Al $3s^2$ $3p^1$, Ga $3d^{10}$ $4s^2$ $4p^1$, S $3s^2$ $3p^4$. In all cases, the band structures, density of states (DOS), and optical properties of the compounds were calculated with the Monkhorst-Pack *k*-point meshes in the Brillouin zone of $3 \times 3 \times 4$ for $CdAl_2S_4$, $4 \times 4 \times 2$ for $HgAl_2S_4$, $3 \times 3 \times 4$ for $CdGa_2S_4$ and $3 \times 3 \times 4$ for $HgGa_2S_4$, respectively.

Furthermore, the length-gauge formalism derived by Aversa and Sipe [35] was performed to calculate the NLO coefficients at a zero frequency limit, and later developed by Zhang et al. Since the two band contributions are proved to be zero under the length-gauge, the static second-order nonlinear coefficients $\chi^{(2)}_{\alpha\beta\gamma}$ can be simplified as:

$$\chi_{\alpha\beta\gamma}{}^{(2)} = \chi_{\alpha\beta\gamma}{}^{(2)}(\mathrm{VE}) + \chi_{\alpha\beta\gamma}{}^{(2)}(\mathrm{VH}) \quad (1)$$

here, $\alpha$, $\beta$, and $\gamma$ are Cartesian components, $\chi^{(2)}_{\alpha\beta\gamma}$ (VE), $\chi^{(2)}_{\alpha\beta\gamma}$ (VH) represent virtual-electron (VE) process and virtual-hole (VH) process, respectively [36,37].

## 3. Results and discussion

### 3.1. Crystal structure

The title compounds belong to defect chalcopyrite (DC) family of $A^{II}B^{III}_2C^{VI}_4$ ($A^{II}$ = Zn, Cd, Hg; $B^{III}$ = Al, Ga, In; $C^{VI}$ = S, Se, Te), and crystallize in the same NCS tetragonal $I\bar{4}$ space group. So we take $HgGa_2S_4$ as an example to describe the crystal structure. As shown in Fig. 1(a), two gallium atoms take different positions in the unit cell, and each cation is coordinated to four S atoms, forming [$HgS_4$] and [$GaS_4$] undistorted tetrahedra. In the structure of the 3D frameworks, all [$GaS_4$] tetrahedra are connected by the vertex-sharing S atoms, as shown in Fig. 1(b). And it also shows that the overall arrangement of [$GaS_4$] tetrahedra nearly aligned in parallel along the [111] direction.

### 3.2. Band gap and electronic structure

A plane-wave pseudopotential CASTEP package based on DFT has been shown to provide the description of band structure and electronic structure. The calculated band gaps are 3.13 eV for $CdAl_2S_4$, 2.21 eV for $HgAl_2S_4$, 2.19 eV for $CdGa_2S_4$ and 1.80 eV for $HgGa_2S_4$, which are well consistent with the experimental results with slightly difference owing to the discontinuity of exchange correlation energy [38]. Since they have similar electronic structures, here we take $HgGa_2S_4$ as a typical example. As shown in Fig. 2(d), the energy levels from approximately −6 to 0 eV in the valence bands are mainly derived from S-3*p*, Hg-5*d*6*s* and Ga-4*s*4*p* orbitals, and the energy levels between nearly 2.5 and 5 eV in the conduction bands are dominated by S-3*p*, Ga-4*s*4*p* and Hg-6s orbitals. The electronic structures indicate that both Hg-S and Ga-S tetrahedra have influences on the changes in band gaps. And a similar electronic structure can be observed among $CdAl_2S_4$, $CdGa_2S_4$ and $HgAl_2S_4$, as shown in Fig. 2(a), (b), (c). In addition, it can be clearly seen that there is a trend of the decrease in gaps from Al to Ga and from Cd to Hg. In fact, the change in cell sizes also provides a possible explanation for the variation in band gaps due to the bigger cell size results in narrower energy level spacing [39]. Different cations will change cell sizes, and the cell sizes are 309.0 $Å^3$ for $HgAl_2S_4$, 310.9 $Å^3$ for $HgGa_2S_4$, 311.5 $Å^3$ for $CdAl_2S_4$, 312.9 $Å^3$ for $CdGa_2S_4$. Larger cell may result in smaller gaps, such phenomenon appears in $AAl_2S_4$ vs. $AGa_2S_4$ (A = Cd, Hg) but not in $CdB_2S_4$ vs. $HgB_2S_4$ (B = Al, Ga). Main reason is that the band gap is also greatly influenced by *dp* hybridization and cation electronegativity besides a structural effect [40]. When the cation substitution occurs in the A (Cd, Hg)-site system, the degree of *dp* hybridization between A (A = Cd, Hg)-*d* and S-*p* orbitals plays a dominant role, which affects the valence band energies and band shifts. Comparing the partial density of states (PDOS) of the Cd-containing with that of the Hg-containing compounds in Fig. 2, *dp* hybridization in $HgB_2S_4$ is much stronger than that in $CdB_2S_4$ which indicates that $HgB_2S_4$ have smaller band gaps than $CdB_2S_4$ (B=Al, Ga), $E_g$ ($CdAl_2S_4$) > $E_g$ ($HgAl_2S_4$), $E_g$ ($CdGa_2S_4$) > $E_g$ ($HgGa_2S_4$). However, for the case of B-site cation substitution, as in $AAl_2S_4$ vs. $AGa_2S_4$ (A = Cd, Hg), the different charge separation caused by cation

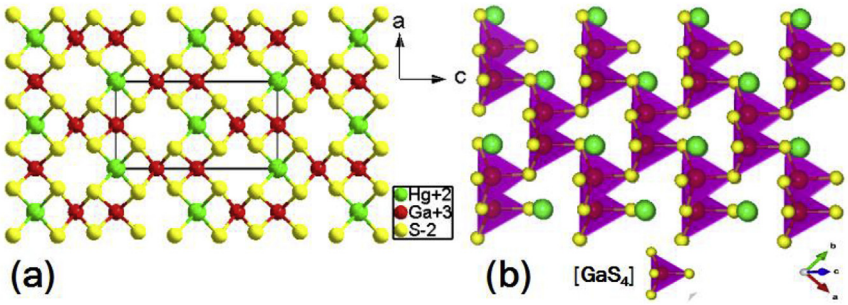


**Fig. 1.** The crystallographic structure for $HgGa_2S_4$.

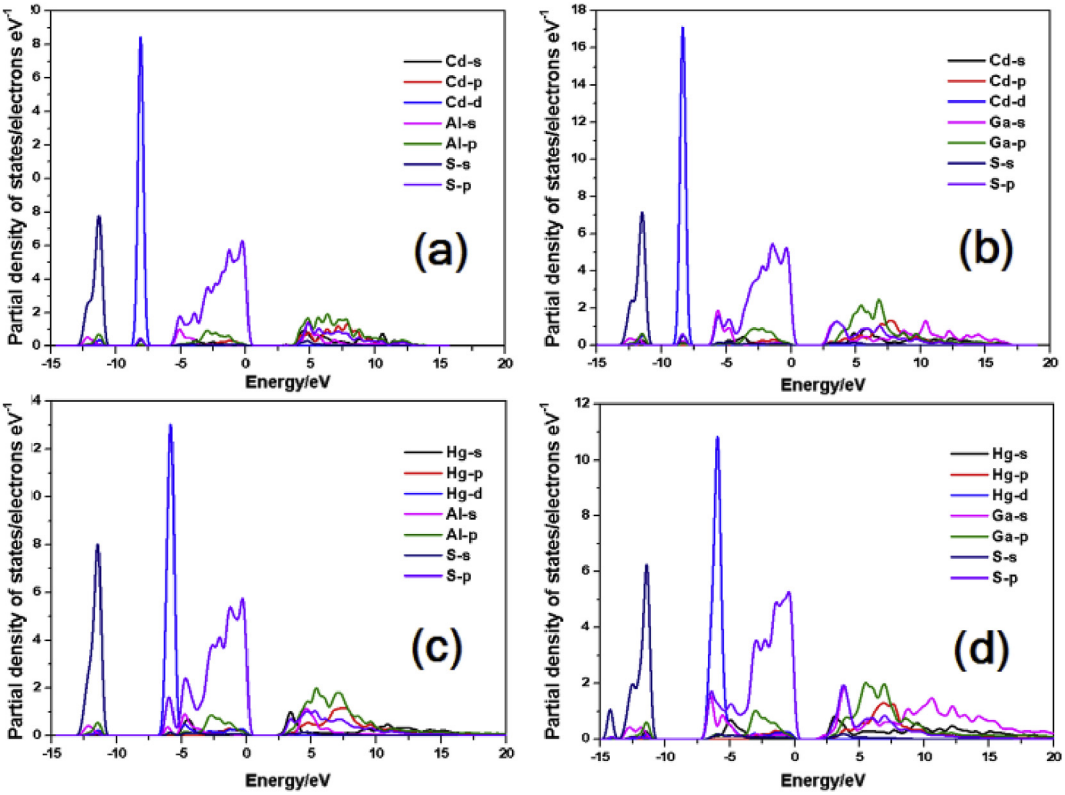


**Fig. 2.** Partial density of states for $CdAl_2S_4$ (a), $CdGa_2S_4$ (b), $HgAl_2S_4$ (c), $HgGa_2S_4$ (d).

electronegativity (1.81 for Ga, and 1.61 for Al) and cell sizes (309.0 Å$^3$ for $HgAl_2S_4$ & 310.9 Å$^3$ for $HgGa_2S_4$, and 311.5 Å$^3$ for $CdAl_2S_4$ & 312.9 Å$^3$ for $CdGa_2S_4$) play a crucial role in the trend of band gap, namely, $E_g$ ($CdAl_2S_4$) > $E_g$ ($CdGa_2S_4$), and $E_g$ ($HgAl_2S_4$) > $E_g$ ($HgGa_2S_4$).

### 3.3. SHG properties

All the title compounds are NCS structures, and the NLO properties were estimated by the first-principles calculation. According to Kleinman's symmetry rule, the investigated compounds have two nonzero independent SHG coefficients due to their $I\bar{4}$space group. Considering that the SHG calculation is highly sensitive to band gaps [39,44], a corrected scissors operator defined as the difference between the calculated and experimental is used to evaluate the optical properties calculation. Table 1 shows the calculated SHG coefficients: $CdAl_2S_4$ ($d_{36} = 7.82$ pm/V, $0.6 \times AgGaS_2$), $HgAl_2S_4$ ($d_{36} = 12.63$ pm/V, $1 \times AgGaS_2$), $CdGa_2S_4$ ($d_{36} = 14.83$ pm/V, $1.1 \times AgGaS_2$), $HgGa_2S_4$ ($d_{36} = 20.59$ pm/V, $1.6 \times AgGaS_2$). The spatial distribution of electronic states making the major contributions to SHG response, namely, the SHG-density [45], was applied to analyze or clarify the effective NLO functional units. SHG-density can be divided into occupied and unoccupied states of Virtual-Electron (VE) and Virtual-Hole (VH), respectively. In consequence, the SHG caused by quantum states can be clearly shown through the SHG-density of occupied or unoccupied states, however, the states do not contribute to SHG will be invisible. In all cases, VE process is analyzed because it dominates the origin of SHG response. Taking $HgGa_2S_4$ as an example in Fig. 3(a and b), S bonding 3*p* orbitals are the major contributor to SHG effect in occupied states, and partially Hg-5d orbitals, the *sp* hybridization between S-3*p* orbitals and Hg-6s orbitals also contribute to SHG effect. Like the occupied states, the unoccupied states where bonding 3*p* orbitals of S are also the dominant contributor, and Ga-4*p* states and Hg-6s states have partially contributions. SHG-densities of $HgAl_2S_4$, $CdAl_2S_4$ and $CdGa_2S_4$ are also shown in Fig. 3(c and d); Fig. 3(e and f); Fig. 3(g and h). Combining SHG-density with electronic structure of title compounds, we conclude that both the interactions between S and B (Al, Ga), S and A (Cd, Hg) contribute to the SHG response. Furthermore, the tetrahedra [$BS_4$] (B = Al, Ga), one of the fundamental NLO- functional units, aligning in parallel are conducive for enhancing the SHG response.

**Table 1**
Calculated SHG coefficients and band gaps for the compounds $CdAl_2S_4$, $HgAl_2S_4$, $CdGa_2S_4$ and $HgGa_2S_4$.

| Compounds | Space group | Band gap (eV) | SHG coefficients $d_{36}$ (pm/V) |
|---|---|---|---|
| $CdAl_2S_4$ | $I\bar{4}$ | 3.13 (Cal.)<br>3.82 (Exp.)[a] | 7.82 (Cal.) |
| $HgAl_2S_4$ | $I\bar{4}$ | 2.21 (Cal.)<br>3.43 (Exp.)[b] | 12.63(Cal.) |
| $CdGa_2S_4$ | $I\bar{4}$ | 2.19 (Cal.)<br>3.44 (Exp.)[c] | 14.83(Cal.) 15.83[d]<br>21.45 (Powder effect.)[e] |
| $HgGa_2S_4$ | $I\bar{4}$ | 1.80 (Cal.)<br>2.84 (Exp.)[d] | 20.59(Cal.) 25.15[d]<br>31.50 (Powder effect.)[d] |

(Cal.) This work;
[a] [41].
[b] [42].
[c] [11].
[d] [11].
[e] [43].

### 3.4. Mechanism in balance on Gap-SHG

(1) Mulliken atomic population analysis

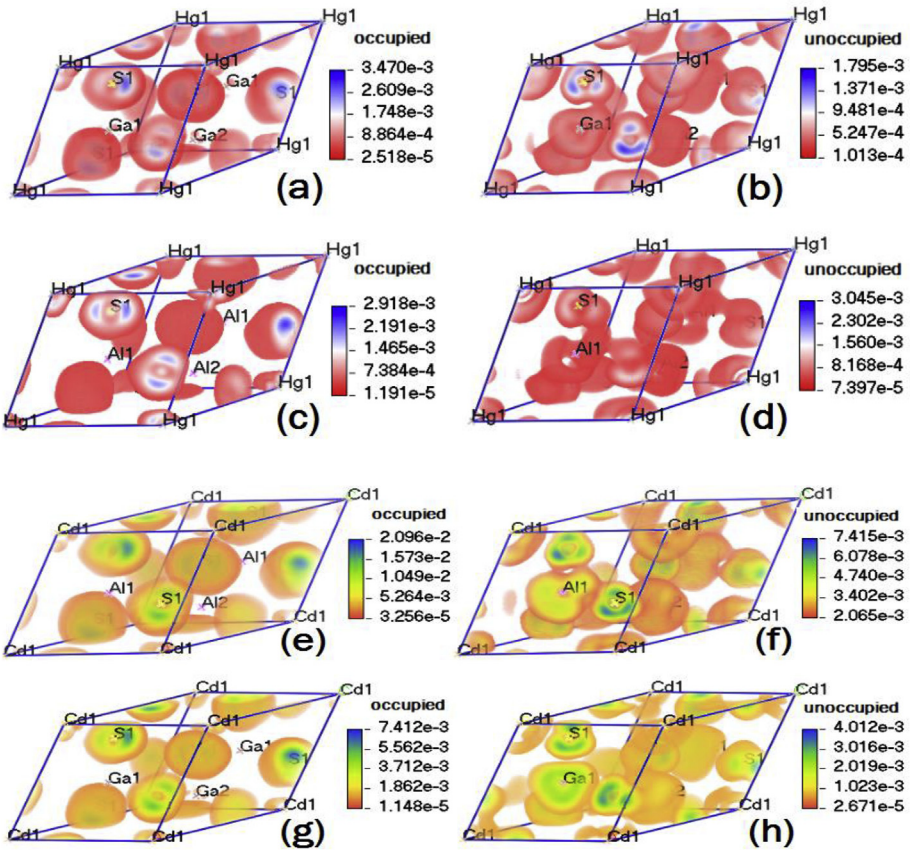


**Fig. 3.** SHG-density of occupied and unoccupied for $HgGa_2S_4$(a, b), $HgAl_2S_4$(c, d), $CdAl_2S_4$(e, f), $CdGa_2S_4$(g, h).

The DC family $AB_2S_4$ (A = Cd, Hg; B = Al, Ga) provides a structural framework to explore the influence of cations on band gaps and SHG properties in a lattice with relatively undistorted tetrahedra structural buildings. In this paper, Mulliken population analysis was performed to get more information about the bonding character and to illuminate the charge transfer among title compounds [45], and the calculated results are listed in Table 2. It is known that, the ionic bonding with a character of larger Mulliken atomic charge and the covalent bonding with a character of smaller Mulliken atomic charge [46]. For charge transfer, there is no distinct difference between Cd-S and Hg-S in the similar systems ($CdAl_2S_4$ vs. $HgAl_2S_4$, $CdGa_2S_4$ vs. $HgGa_2S_4$) but a marked difference between Al-S and Ga-S, which indicates a character of relatively stronger covalent bonding between B (Al, Ga)-S [47]. To better clarify the bonding behavior of the compounds, the calculated Mulliken overlap populations Q are also listed in Table 2, compared with the overlap population of Ga-S (0.48–0.52) in $CdGa_2S_4$, there is a greater value of Al-S (0.61) in $CdAl_2S_4$, and this phenomenon can also be observed in $HgGa_2S_4$ (0.52–0.54) and $HgAl_2S_4$ (0.57–0.59). It further indicates that the interaction of Ga-S is weaker than that Al-S. Meanwhile, A (Cd, Hg)-S is characterized by a slightly smaller overlap population, which further indicates the weaker covalent bonding than that B (Al, Ga)-S.

**Table 2**
Mulliken charge (|e|), bond population (Q) for $CdAl_2S_4$, $HgAl_2S_4$, $CdGa_2S_4$ and $HgGa_2S_4$.

| Compounds | Species | Charge (e) | Bond | Bond Length (Å) | Population (Q) |
|---|---|---|---|---|---|
| $CdAl_2S_4$ | Cd | 0.99 | Cd-S | 2.53228 | 0.30 |
| | Al | 0.70–0.75 | Al-S | 2.24934–2.25541 | 0.61 |
| | S | −0.61 | / | / | / |
| $HgAl_2S_4$ | Hg | 0.64 | Hg-S | 2.52448 | 0.28 |
| | Al | 0.79–0.83 | Al-S | 2.27339–2.33243 | 0.57–0.59 |
| | S | −0.57 | / | / | / |
| $CdGa_2S_4$ | Cd | 0.62 | Cd-S | 2.43661 | 0.45 |
| | Ga | 0.55–0.72 | Ga-S | 2.29898–2.37337 | 0.48–0.52 |
| | S | −0.47 | / | / | / |
| $HgGa_2S_4$ | Hg | 0.33 | Hg-S | 2.52894 | 0.40 |
| | Ga | 0.59–0.73 | Ga-S | 2.28082–2.28334 | 0.52–0.54 |
| | S | −0.41 | / | / | / |

(2) Influence of cations on S

To further explore the influences of different cations on the electronic structure of S, we investigated the electronic structure differences of S-3*p* orbitals for all compounds. According to the theory of molecular orbital, the microscopic energy gap between the anti-bonding and bonding states of two atoms $\Delta E$ is closely related to the orbital energies of two atoms (atom 1 and 2), $E_1$ and $E_2$. And $\Delta E$ can be written as:

$$\Delta E = \sqrt{(E_2 - E_1)^2 + 4\beta^2} \quad (2)$$

here $\beta$ is the exchange integral, since the orbital energies of atoms agree well with the bandwidth of orbitals [48]. Fig. 4(a) clearly shows the order of the bandwidth for S-3*p* orbitals: $HgGa_2S_4$ (6.0 eV) > $HgAl_2S_4$ (5.6 eV); $CdGa_2S_4$ (5.3 eV) > $CdAl_2S_4$ (4.9 eV). One can see that the bandwidth of S-3*p* orbitals in $AGa_2S_4$ is wider than that in $AAl_2S_4$ (A = Cd, Hg), that is to say, the S-3*p* orbitals in $CdAl_2S_4$ are slightly localized than that in $CdGa_2S_4$, accordingly, the S-3*p* orbitals in $HgAl_2S_4$ are also mildly localized than that in

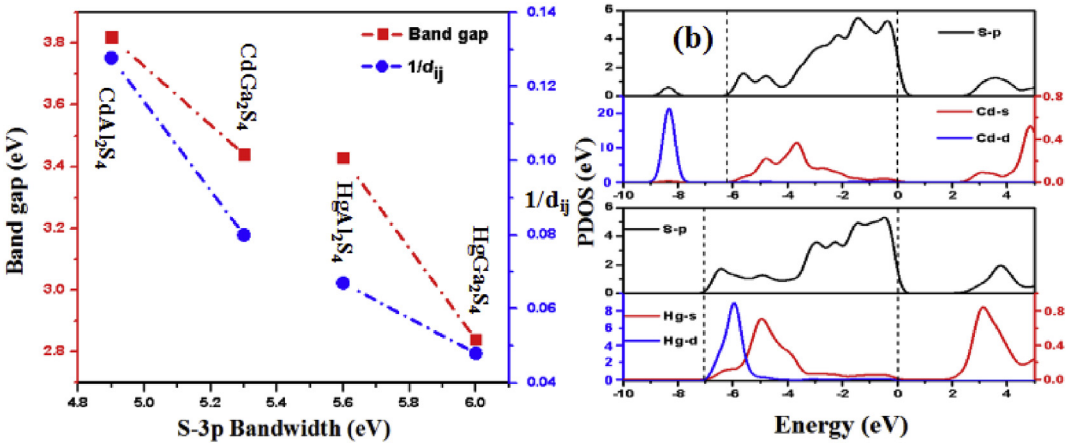


**Fig. 4.** The relationship among band gap, SHG coefficients and bandwidth of the S-3*p* orbital for $CdAl_2S_4$, $CdGa_2S_4$, $HgAl_2S_4$, and $HgGa_2S_4$ (a); *sp*/*dp* hybridization between A (Cd, Hg)-*s*/*d* and S-*p* in $CdGa_2S_4$ and $HgGa_2S_4$ (b).

$HgGa_2S_4$. Noting that there is an increase of 0.4 eV in bandwidth of S-3*p* orbitals from Al to Ga and there is also a trend of increase of 0.7 eV from Cd to Hg. Coincidentally, it is in well agreement with the trend of increase of SHG coefficients. This can be explained that the bonding and antibonding behaviors between Ga and S are different between Al and S due to the distinction of electronegativity. This is why S-3*p* orbitals in $HgAl_2S_4$ are more localized than that in $HgGa_2S_4$, and it works the same for $CdAl_2S_4$ and $CdGa_2S_4$. Comparing $HgGa_2S_4$ and $HgAl_2S_4$, the delocalization degree of S-3*p* orbital is related to the bonding-antibonding energy, which results in a decrease of the band gap from Eq. (2). We conclude that both A-site and B-site cations influence the bandwidth of S-3*p* orbitals, which subsequently impacts other important properties such as the SHG effect.

Furthermore, the SHG effect of $HgAl_2S_4$ is stronger than $CdAl_2S_4$, since the angular momentum difference between *d*-orbitals and *p*-orbitals is also $\hbar$, the differences of calculated PDOS between $HgAl_2S_4$ and $CdAl_2S_4$ reveals that: the *p*-orbitals of S and *d*-orbitals of Hg also have a hybridization in energy range [-6.5, −5] eV, while there is no *dp* hybridization between Cd and S, thus, the stronger SHG effect can be explained from the *dp* hybridization. In addition, Fig. 4(b) shows that the *sp* hybridization between Hg and S in $HgGa_2S_4$ also make a contribution at a considerable energy level in the valence bands. And the SHG effect of $CdGa_2S_4$ is stronger than that $CdAl_2S_4$ can also be illuminated by the differences of bandwidth for S-3*p* orbitals [47].

## 4. Conclusion

In summary, the properties of four metal chalcogenides are investigated in the view of the first-principles calculation. We conclude that the *dp* hybridization, size effect and cation electronegativity induce the changes of band gaps. The differences of NLO property among four compounds are affected by the synergism of charge-transfer energy, the interactions between A(Cd, Hg)/B(Al, Ga) and S. Besides, the cations influence the bonding-antibonding energy of A(Cd, Hg)/B(Al, Ga)-S orbitals, which is captured by the bandwidth of S-3*p* in the valence bands. As Al atoms are replaced by Ga atoms, that is the more delocalization of S-3*p* orbitals which offers the same tendency of NLO properties. From the calculation, it can be seen that B(Al, Ga)-S units have more contributions to SHG effect, and can be as superior NLO functional units. In the further research, one can assemble such superior NLO functional units to design new IR NLO materials with good performance.

## Acknowledgments

This work is supported by the National Natural Science Foundation of China (Grant No. 11564038). MHL is grateful for the database service provided by NCHC (Taiwan) and computer equipment donated by KeyWin Inc.

## References

[1] D.M. Burland, R.D. Miller, C.A. Walsh, 2nd-order nonlinearity in poled-polymer systems, Chem. Rev. 94 (1994) 31–75.
[2] (a) P. Becker, Borate materials in nonlinear optics, Adv. Mater. 10 (1998) 979–992;
(b) A.S. Hassanien, K.A. Aly, Alaa. A. Akl, Study of optical properties of thermally evaporated ZnSe thin films annealed at different pulsed laser powers, J. Alloys Compd. 685 (2016) 733–742.
[3] H.Y. Chang, S.H. Kim, P.S. Halasyamani, K.M. Ok, Alignment of lone pairs in a new polar material: synthesis, characterization, and functional properties of $Li_2Ti(IO_3)_6$, J. Am. Chem. Soc. 40 (2009) 2426–2427.
[4] T.T. Tran, H.W. Yu, J.M. Rondinelli, K.R. Poeppelmeier, P.S. Halasyamani, Deep ultraviolet nonlinear optical materials, Chem. Mater. 28 (2016) 5238–5258.
[5] (a) C.T. Chen, B.C. Wu, A.D. Jiang, G.M. You, A new-type ultraviolet SHG crystal - $\beta$-$BaB_2O_4$, Sci. Sin Ser. B 28 (1985) 235–243;
(b) C.T. Chen, Y.C. Wu, A.D. Jiang, B.C. Wu, G.M. You, R.K. Li, Z.J. Lin, New nonlinear-optical crystal: $LiB_3O_5$, J. Opt. Soc. Am. B 6 (1989) 616–621;
(c) C.T. Chen, G.L. Wang, X.Y. Wang, Z.Y. Xu, Deep-UV nonlinear optical crystal $KBe_2BO_3F_2$ - discovery, growth, optical properties and applications, Appl. Phys. B 97 (2009) 9–25;
(d) S.G. Zhao, P.F. Gong, L. Bai, X. Xu, S.Q. Zhang, Z.H. Sun, Z.S. Lin, M.C. Hong, C.T. Chen, J.H. Luo, Beryllium-free $Li_4Sr(BO_3)_2$ for deep-ultraviolet nonlinear optical applications, Nat. Commun. 5 (2014) 4019;
(e) H.P. Wu, S.L. Pan, K.R. Poeppelmeier, H.Y. Li, D.Z. Jia, Z.H. Chen, X.Y. Fan, Y. Yang, J.M. Rondinelli, H.S. Luo, $K_3B_6O_{10}Cl$: a new structure analogous to perovskite with a large second harmonic generation response and deep uv absorption edge, J. Am. Chem. Soc. 133 (2011) 7786–7790.
[6] (a) G.H. Zou, L. Huang, N. Ye, C.S. Lin, W.D. Cheng, H. Huang, $CsPbCO_3F$: a strong second-harmonic generation material derived from enhancement via *p*-$\pi$ Interaction, J. Am. Chem. Soc. 135 (2013) 18560–18566;
(b) L. Huang, Q. Wang, C.S. Lin, G.H.D.J. Gao, J. Bi, N. Ye, Synthesis and characterization of a new beryllium-free deep-ultraviolet nonlinear optical material: $Na_2GdCO_3F_3$, J. Alloys Compd. 724 (2017) 1057–1063.
[7] M. Bass, H.H. Barrett, Laser-induced damage probability at 1.06 μm and 0.69 μm, Appl. Opt. 12 (1973) 690–699.
[8] B.B. Zhang, G.Q. Shi, Z.H. Yang, F.F. Zhang, S.L. Pan, Fluorooxoborates: beryllium-free deep-ultraviolet nonlinear optical materials without layered growth, Angew. Chem. Int. Ed. 56 (2017) 3916–3919.
[9] (a) G.Q. Shi, Y. Wang, F.F. Zhang, B.B. Zhang, Z.H. Yang, X.L. Hou, S.L. Pan, K.R. Poeppelmeier, Finding the next deep-ultraviolet nonlinear optical material: $NH_4B_4O_6F$, J. Am. Chem. Soc. 139 (2017) 10645–10648;
(b) Y. Wang, B.B. Zhang, Z.H. Yang, S.L. Pan, Cation-tuned synthesis of fluorooxoborates: towards optimal deep-ultraviolet nonlinear optical materials, Angew. Chem. Int. Ed. 57 (2018) 2150–2154;
(c) X.F. Wang, Y. Wang, B.B. Zhang, F.F. Zhang, Z.H. Yang, S.L. Pan, $CsB_4O_6F$: a congruent-melting deep-ultraviolet nonlinear optical material by combining superior functional units, Angew. Chem. Int. Ed. 129 (2017) 14307–14311.
[10] I. Chung, M.G. Kanatzidis, Metal chalcogenides: a rich source of nonlinear

optical materials, Chem. Mater. 26 (2014) 849–869.
[11] (a) F. Liang, L. Kang, Z.S. Lin, Y.C. Wu, C.T. Chen, Analysis and prediction of mid-ir nonlinear optical metal sulfides with diamond-like structures, Coord. Chem. Rev. 333 (2017) 57–70;
(b) S.P. Guo, Y. Chi, G.C. Guo, Recent achievements on middle and far-infrared second-order nonlinear optical materials, Coord. Chem. Rev. 333 (2017) 44–57.
[12] (a) G.D. Boyd, H. Kasper, J.H. Mcfee, Linear and nonlinear optical properties of $AgGaS_2$, $CuGaS_2$, and $CuInS_2$, and theory of the wedge technique for the measurement of nonlinear coefficients, IEEE J. Quant. Electron. 7 (1971) 563–573;
(b) G.D. Boyd, H. Kasper, J. Mcfee, F. Storz, Linear and nonlinear optical properties of some ternary selenides, IEEE J. Quant. Electron. 8 (1972) 900–908.
[13] G.D. Boyd, E. Buehler, F.G. Storz, Linear and nonlinear optical properties of $ZnGeP_2$ and CdSe, Appl. Phys. Lett. 18 (1971) 301–304.
[14] (a) Y. Huang, X.G. Meng, P.F. Gong, Z.S. Lin, X.G. Chen, J.G. Qin, Study on $K_2SbF_2Cl_3$ as a new mid-ir nonlinear optical material: new synthesis and excellent properties, J. Mater. Chem. C 3 (2015) 9588–9593;
(b) K. Feng, W.L. Yin, Z.H. Lin, J.Y. Yao, Y.C. Wu, Five new chalcohalides, $Ba_3GaS_4X$ (X = Cl, Br), $Ba_3MSe_4Cl$ (M = Ga, In), and $Ba_7In_2Se_6F_8$: syntheses, crystal structures, and optical properties, Inorg. Chem. 52 (2013) 11503–11508.
[15] K. Wu, B.B. Zhang, Z.H. Yang, S.L. Pan, New compressed chalcopyrite-like $Li_2BaM^{IV}Q_4$ ($M^{IV}$ = Ge, Sn; Q = S, Se): promising infrared nonlinear optical materials, J. Am. Chem. Soc. 139 (2017) 14885–14888.
[16] (a) J.H. Zhang, D.J. Clark, A. Weiland, S.S. Stoyko, Y.S. Kim, J.I. Jang, J.A. Aitken, $Li_2CdGeSe_4$ and $Li_2CdSnSe_4$: biaxial nonlinear optical materials with strong infrared second-order responses and laser-induced damage thresholds influenced by photoluminescence, Inorg. Chem. Front. 4 (2017) 1472–1484;
(b) F. Liang, L. Kang, Z.S. Lin, Y.C. Wu, Mid-infrared nonlinear optical materials based on metal chalcogenides: structure-property relationship, Cryst. Growth Des. 17 (2017) 2254–2289;
(c) K. Wu, Z.H. Yang, S.L. Pan, The first quaternary diamond-like semiconductor with 10-membered $LiS_4$ rings exhibiting excellent nonlinear optical performances, Chem. Commun. 53 (2017) 3010–3013.
[17] I. Chung, J.H. Song, J.I. Jang, A.J. Freeman, M.G. Kanatzidis, $Na_2Ge_2Se_5$: a highly nonlinear optical material, J. Solid State Chem. 195 (2012) 161–165.
[18] A.H. Reshak, S. Auluck, I.V. Kityk, Several features of nonlinear optical susceptibilities of $LiGaX_2$ (X = S, Se) ternary compounds, J. Alloys Compd. 473 (2009) 20–24.
[19] L. Isaenko, I. Vasilyeva, A. Merkulov, A. Yelisseyev, S. Lobanov, Growth of new nonlinear crystals $LiMX_2$ (M = Al, In, Ga; X = S, Se, Te) for the mid-ir optics, J. Cryst. Growth 275 (2005) 217–223.
[20] J.W. Lekse, M.A. Moreau, K.L. Mcnerny, J. Yeon, P.S. Halasyamani, J.A. Aitken, Second-harmonic generation and crystal structure of the diamond-like semiconductors $Li_2CdGeS_4$ and $Li_2CdSnS_4$, Inorg. Chem. 48 (2009) 7516–7518.
[21] G.M. Li, Y. Chu, Z.X. Zhou, From $AgGaS_2$ to $Li_2ZnSiS_4$: realizing impressive high laser damage threshold together with large second-harmonic generation response, Chem. Mater. 30 (2018) 602–606.
[22] C. Li, W.L. Yin, P.F. Gong, X.S. Li, M.L. Zhou, A. Mar, Z.S. Lin, J.Y. Yao, Y.C. Wu, C.T. Chen, Trigonal planar $[HgSe_3]^{4-}$ unit: a new kind of basic functional group in ir nonlinear optical materials with large susceptibility and physicochemical stability, J. Am. Chem. Soc. 47 (2016) 6135–6138.
[23] Y.Y. Li, B.X. Li, G. Zhang, L.J. Zhou, H. Lin, J.N. Shen, C.Y. Zhang, L. Chen, L.M. Wu, Syntheses, characterization, and optical properties of centrosymmetric $Ba_3(BS_3)_{1.5}(MS_3)_{0.5}$ and noncentrosymmetric $Ba_3(BQ_3)(SbQ_3)$, Inorg. Chem. 54 (2015) 4761–4767.
[24] (a) A. Weiland, J.H. Zhang, D.J. Clark, J.A. Brant, C.W. Sinagra, Y.S. Kim, J.L. Jang, J.A. Aitken, Infrared nonlinear optical properties of lithium-containing diamond-like semiconductors $Li_2ZnGeSe_4$ and $Li_2ZnSnSe_4$, Dalton Trans. 44 (2015) 10102–10104;
(b) J.A. Brant, D.J. Clark, Y.S. Kim, J.I. Jang, J.H. Zhang, J.A. Aitken, $Li_2CdGeS_4$, a diamond-like semiconductor with strong second-order optical nonlinearity in the infrared and exceptional laser damage threshold, Chem. Mater. 26 (2014) 3045–3048.
[25] K. Wu, Z.H. Yang, S.L. Pan, $Na_2Hg_3M_2S_8$ (M = Si, Ge, and Sn): new infrared nonlinear optical materials with strong second harmonic generation effects and high laser-damage thresholds, Chem. Mater. 28 (2017) 2795–2801.
[26] Y. Huang, X.G. Meng, P.F. Gong, Z.S. Lin, X.G. Chen, J.G. Qin, Study on $K_2SbF_2Cl_3$ as a new mid-ir nonlinear optical material: new synthesis and excellent properties, J. Mater. Chem. C 3 (2015) 9588–9593.
[27] W. Kohn, Nobel Lecture: electronic structure of matter-wave functions and density functionals, Rev. Mod. Phys. 71 (1999) 1253–1266.
[28] L. Kang, M.L. Zhou, J.Y. Yao, Z.S. Lin, Y.C. Wu, C.T. Chen, Metal thiophosphates with good mid-infrared nonlinear optical performances: a first-principles prediction and analysis, J. Am. Chem. Soc. 137 (2015) 13049–13059.
[29] S.J. Clark, M.D. Segall, C.J. Pickard, P.J. Hasnip, M.I.J. Probert, K. Refson, M.C. Payne, First principles methods using castep, Z. Kristallogr. 220 (2005) 567–570.
[30] J.P. Perdew, W. Yue, Accurate and simple density functional for the electronic exchange energy: generalized gradient approximation, Phys. Rev. B 33 (1986) 8800–8802.
[31] M. Ernzerhof, G.E. Scuseria, Assessment of the Perdewe-Burkee-Ernzerhof exchange-correlation functional, J. Chem. Phys. 110 (1999) 5029–5036.
[32] A.M. Rappe, K.M. Rabe, E. Kaxiras, J.D. Joannopoulos, Optimized pseudopotentials, Phys. Rev. B 41 (1990) 1227–1230.
[33] J.S. Lin, A. Qteish, M.C. Payne, V. Heine, Optimized and transferable nonlocal separable *ab-initio* pseudopotentials, Phys. Rev. B 47 (1993) 4174–4180.
[34] K. Liu, H.Q. Fan, P.R. Ren, C. Yang, Structural, electronic and optical properties of $BiFeO_3$ studied by first-principles, J. Alloys Compd. 509 (2011) 1901–1905.
[35] C. Aversa, J.E. Sipe, Nonlinear optical susceptibilities of semiconductors: results with a length-gauge analysis, Phys. Rev. B 52 (1995) 14636–14645.
[36] J. Lin, M.H. Lee, Z.P. Liu, C. Chen, C.J. Pickard, Mechanism for linear and nonlinear optical effects in $\beta$-$BaB_2O_4$ crystals, Phys. Rev. B 93 (1999) 9717–9723.
[37] B.B. Zhang, M.H. Lee, Z.H. Yang, Q. Jing, S.L. Pan, M. Zhang, H.P. Wu, X. Su, C.S. Li, Simulated pressure-induced blue-shift of phase-matching region and nonlinear optical mechanism for $K_3B_6O_{10}X$ (X = Cl, Br), Appl. Phys. Lett. 106 (2015) 992–996.
[38] M.K.Y. Chan, G. Ceder, Efficient band gap prediction for solids, Phys. Rev. Lett. 105 (2010) 196403.
[39] (a) M.H. Lee, C.H. Yang, J.H. Jan, Band-resolved analysis of nonlinear optical properties of crystalline and molecular materials, Phys. Rev. B 70 (2004) 155–163;
(b) Y.Z. Sun, Z.H. Yang, D.W. Hou, S.L. Pan, Theoretical investigation on the balance between large band gap and strong SHG response in $BMO_4$ (M = P and As) crystals, RSC Adv. 7 (2017) 2804–2809.
[40] J.E. Jaffe, A. Zunger, Theory of the band-gap anomaly in $ABC_2$ chalcopyrite semiconductors, Phys. Rev. B 29 (1984) 1882–1906.
[41] A. Eifler, J.D. Hecht, V. Riede, G. Lippold, W. Schmitz, G. Krauss, V. Kramer, W. Grill, Infrared and Raman study of lattice vibration of $CdAl_2Se_4$ and $CdAl_2S_4$ single crystals, J. Phys. Condens. Matter 11 (1999) 4821–4832.
[42] X.S. Jiang, W.R.L. Lambrecht, Electronic band structure of ordered vacancy defect chalcopyrite compounds with formula $II\text{-}III_2\text{-}VI_4$, Phys. Rev. B 69 (2004) 1129–1133.
[43] B.F. Levine, C.G. Bethea, H.M. Kasper, Nonlinear optical susceptibility of thiogallate $CdGa_2S_4$, IEEE J. Quant. Electron. QE10 (1974) 904–906.
[44] B.B. Zhang, Z.H. Yang, Y. Yang, M.H. Lee, S.L. Pan, Q. Jing, X. Su, $p$-($p$, $\pi^*$) interaction mechanism revealing and accordingly designed new member in deep-ultraviolet NLO borates $Li_nM_{n-1}B_{2n-1}O_{4n-2}$ (M = Cs/Rb, n = 3, 4, 6), J. Mater. Chem. C 2 (2014) 4133–4141.
[45] D.W. Hou, Z.H. Yang, S.L. Pan, Electronic, bond order, linear optical properties of series of alkalimetal P-O-P linkage borophosphates, J. Alloys Compd. 706 (2017) 589–595.
[46] X. Su, Z.H. Yang, M.H. Lee, S.L. Pan, Y. Wang, X.Y. Fang, Z.J. Huang, B.B. Zhang, Evidence of "new hot spots" from determining the nonlinear optical behavior of materials: mechanism studies on vanadium borate crystal $Na_3VO_2B_6O_{11}$, Phys. Chem. Chem. Phys. 17 (2015) 5338–5344.
[47] Z. Li, Q. Liu, Y. Wang, T. Iitaka, H.B. Su, T. Tohyama, Z.H. Yang, S.L. Pan, Second-harmonic generation in noncentrosymmetric phosphates, Phys. Rev. B 96 (2017), 035205.
[48] B.H. Lei, Q.R. Kong, Z.H. Yang, Y. Yang, Y. Wang, S.L. Pan, Hierarchized band gap and enhanced optical responses of trivalent rare-earth metal nitrates due to (d-p)π conjugation interactions, J. Mater. Chem. C 4 (2016) 6295–6301.